Materials Research Express

PAPER

Preparation and properties of DLC/MoS_2 multilayer coatings for high humidity tribology

RECEIVED
5 April 2016

REVISED
11 May 2016

ACCEPTED FOR PUBLICATION
12 May 2016

PUBLISHED
17 June 2016

Xiaoyu Zhao[1,3], **Zhibin Lu**[1], **Guizhi Wu**[1], **Guangan Zhang**[1,4], **Liping Wang**[1,2,4] **and Qunji Xue**[1]

[1] State Key Laboratory of Solid Lubrication, Lanzhou Institute of Chemical Physics, Chinese Academy of Sciences, Lanzhou 730000, People's Republic of China
[2] Key Laboratory of Marine Materials and Related Technologies, Key Laboratory of Marine Materials and Protective Technologies of Zhejiang Province, Ningbo Institute of Materials Technology and Engineering, Chinese Academy of Sciences, Ningbo 315201, People's Republic of China
[3] Graduate University of Chinese Academy of Sciences, Beijing 100049, People's Republic of China
[4] Authors to whom any correspondence should be addressed.

E-mail: gazhang@licp.cas.cn **and** lpwang@licp.cas.cn

Keywords: DLC, MoS_2, humidity, multilayer, tribology

Abstract

The DLC/MoS_2 multilayer coatings with different modulus ratios were deposited by magnetron sputtering in this study. The morphology, structure, composition, mechanical properties and tribological properties were investigated using several analytical techniques (FESEM, AFM, TEM, AES, XPS, nanoindentation and high humidity tribological test). The results showed that the well-defined multilayer coatings were composed of densely packed particles in which many nanocrystallines with some kinds of defects were distributed in matrix. The incorporation of oxygen into the lattice led to the degraded chemical stability. The coating's hardness and elastic modulus were almost in the same range. Moderate improvement on the high humidity tribological properties were obtained, which was important for the extension of the service life of MoS_2 in humid air.

1. Introduction

Molybdenum disulfide (MoS_2) is one of the prototypical two-dimensional (2D) layered materials, where Mo atoms are sandwiched between layers of S atoms [1]. Atoms within each layer are kept together by covalent bonds, while adjacent layers are held together by weak van der Waals forces which lead to easily shear between basal planes of MoS_2 and a resultant excellent lubricity [1, 2]. The outstanding lubrication property of MoS_2 endows itself good performance in vacuum and space environments [1, 3]. However, ground storage is inevitable before launch in space projects and it will deteriorate the lubricated parts for subsequent use in space [4, 5]. When stored in terrestrial atmosphere, the sensitivity of MoS_2 to moisture results in the formation of MoO_3 with increasing shear strength and a degraded endurance life [6, 7]. Finally, a decreased endurance life is expected for aerospace applications, which may bring about wrong evaluation of service life and serious consequences.

Researches of improving the wear performance of MoS_2 in atmospheric condition are in long-running, where changing the orientation of crystalline, addition of other materials and fabricating double-layer or multilayer coatings are the main subjects [1, 3, 6, 8–10]. One of the successful examples is the development of Ti-doped MoS_2 film, known as MoST, which shows more stable friction coefficient and longer wear life than pure MoS_2 film in humid condition, thus brings itself a promising application in dry drilling and machining [11, 12]. Moreover, the combination of diamond-like carbon (DLC) and MoS_2 has great potential to improve the performance of MoS_2 in atmosphere environment [9]. DLC has been used as protective coatings in many applications because of its low friction, high wear resistance, hardness and chemical inertness [13]. However, hydrogen-free DLC coatings generally exhibit high friction because of the strong adhesion which is attributed to the interaction of covalent σ bonds under ultra-high vacuum (UHV) sliding condition and low friction resulting from the passivation of σ bonds in humid air [14]. Moreover, multilayer structure with soft and hard materials

Table 1. Design parameters of DLC/MoS_2 multilayer and MoS_2 monolayer coatings.

Sample	Modulation ratio	Periodic Thickness (nm)	DLC Deposition time (s)	DLC Thickness (nm)	MoS_2 Deposition time (s)	MoS_2 Thickness (nm)	Total Thickness (nm)
S3	1:3	100	296	25	805	75	1000
S5	1:5	100	197	16.7	894	83.3	1000
S7	1:7	100	148	12.5	939	87.5	1000
S9	1:9	100	118	10	966	90	1000
MoS_2	—	—	—	—	10 730	1000	1000

can further enhance the wear resistance [15]. Therefore, a multilayer structure of DLC and MoS_2 coating is designed to explore the possibility of improved humidity resistant property of MoS_2.

This paper reports on a series of DLC/MoS_2 multilayer coatings deposited on Si wafer and 304 stainless steel by magnetron sputtering. The morphology, microstructure, composition, mechanical properties and tribological properties were investigated. A reduced humidity sensitivity and improved wear resistance of MoS_2 were observed, suggesting potential candidates for aerospace industries.

2. Experimental details

DLC/MoS_2 multilayer and MoS_2 monolayer coatings were deposited by Teer UDP 650 closed-field unbalanced magnetron sputtering system employing four targets. One C target, one MoS_2 target and two Cr targets were used during sputtering. Substrates including Si (100) wafer and 304 stainless steel were ultrasonically cleaned by acetone and ethanol for 15 min subsequently before mounting in the chamber. After the chamber was pumped to less than 1×10^{-3} Pa, substrates and targets were cleaned with Ar^+ ions for 15 min to remove the surface contamination. During the deposition processes, the argon flow rate was kept at 16 sccm. To improve the adhesion to substrates, a Cr interlayer was deposited prior to the deposition of multilayers with a sputtering current 3.0 A for 400 s, followed by a gradient interlayer. During the deposition of DLC layer, a small number of Cr was introduced to reduce the high residual stress and increase the toughness. The sputtering current was 3.5 A for C target, while for Cr target the current was 0.38 A. The target current of MoS_2 was 0.8 A during the deposition of MoS_2 layer. A series of DLC/MoS_2 multilayer coatings about 1000 nm were deposited through alternately changing the target currents. Table 1 depicts the design parameters of DLC/MoS_2 multilayer coatings with various modulation ratios and corresponding deposition times. Additionly, a MoS_2 monolayer coating with a thickness of 1000 nm was deposited as reference sample.

The surface morphology and cross-section structure of coatings were investigated by Hitachi SU8020 field-emission scanning electron microscope (FESEM). Moreover, the detailed morphologies of the coatings were measured by Benyuan CSPM4000 atomic force microscopy (AFM). The crystalline structure was characterized by glancing incidence x-ray diffraction (GIXRD, Philips X'Pert Pro) operating with Cu Kα radiation at 1° angle of incidence. In addition, one cross-section was further examined by FEI Tecnai F30 tansmission electron microscope (TEM) to obtain the information of microstructure. Elemental depth profiling of selected as-deposited DLC/MoS_2 multilayer coating was performed by Auger electron spectroscopy (AES, PHI-700, ULVAC-PHI, Japan). The elastic modulus and hardness of coatings were measured by MTS NANO G200 nanoindentation tester with six measurements in each sample.

Considering the sensitivity of MoS_2 to moisture, a survey of changes in chemical state and composition is essential. Damp heat test (80% relative humidity at 40 °C, 720 h) was carried out to investigate the stability of coatings and the oxidative parts. X-ray photoelectron spectroscopy (XPS) was performed by a VG ESCALAB 210 spectrometer to investigate the changes in coatings before and after the damp heat test.

The tribological performance was evaluated against a GCr15 ball of 4 mm diameter under a constant load of 2 N. The tests were conducted at room temperature and at 90 ± 5% relative humidity by using a reciprocating type ball-on-disk tribometer (CSM, Tribo-S-D-0000). The sliding frequency, amplitude and reciprocating cycle number were maintained at 5 Hz, 5 mm and 20 000 cycles, respectively. After wear tests, the wear volumes were measured by Alpha-Step D-100 profilometer. Raman experiments were carried out to investigate the differences of as-deposited coatings, wear tracks and wear scars using a LabRameHR800 Jobin-Yvon spectrometer with wavelength of 532 nm as excitation source. The wear tracks and wear scars on the balls were observed by Tescan Mira3 SEM equipped with an Energy Dispersive Spectrometer (EDS).

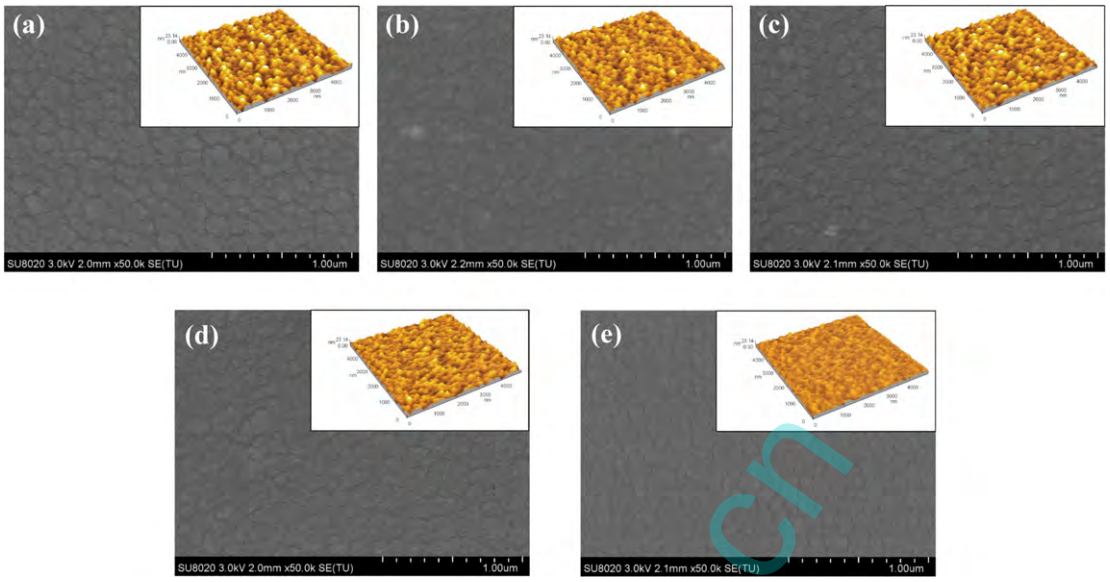

Figure 1. SEM and AFM surface morphologies of the as-deposited coatings: (a) S3—DLC/MoS_2 = 1:3; (b) S5—DLC/MoS_2 = 1:5; (c) S7—DLC/MoS_2 = 1:7; (d) S9—DLC/MoS_2 = 1:9; (e) MoS_2—MoS_2 monolayer coating.

3. Results and discussion

3.1. Morphology and structure

Figure 1 shows the surface morphologies of DLC/MoS_2 multilayer and MoS_2 monolayer coatings measured by FESEM and AFM. All coatings display a densely cluster shape morphology. Uniformly distributed particles can be clearly seen in these figures. The inserted AFM topographic images show three dimensional views of coatings, of which scanning area is 5 μm × 5 μm. The images display a homogeneous topography with hills and valleys of different heights and distances. Whereas a roughness average (Ra) of 1.41 nm was determined for the MoS_2 monolayer coating, the Ra of multilayer coatings were measured to be 3.65 nm, 2.86 nm, 3.23 nm and 2.68 nm for S3, S5, S7 and S9, respectively. The film roughness is mainly determined by the size and of the aggregated MoS_2 particles and the preferred orientation of MoS_2 crystals because of the amorphous property of DLC. The greater the aggregation and the preferred orientation of the MoS_2, the higher the Ra.

The cross-sectional images of all coatings are presented in figure 2. The multilayer coatings show well-defined layered structure with interfaces between adjacent layers easily distinguished. As indicated by arrows and texts in the pictures, the black zones are DLC layers and the grey zones are MoS_2 layers except the interlayers at the bottom. The interlayers are columnar structure, whereas the DLC layers are featureless and MoS_2 layers are composed of densely packed particles.

The GIXRD patterns of all samples are depicted in figure 3. Coatings with different modulus ratios and MoS_2 monolayer coating have same preferential orientations which only differ slightly in intensity, along with diffuse peaks from other reflection groups. The scattering angle is about 12.65° which is inconsistent with the (002) reflection of 2H-MoS_2 (14.378°) and/or the (003) reflection of 3R-MoS_2 (14.533°) [16]. Generally, this peak is assigned to (002) basal plane diffraction peak and the position shift arises from lattice expansion which is common in sputter deposited coatings [17]. Defects like vacancies, impurities and dislocations generate locally strong interactions between MoS_2 layers and inhibit ordered growth due to the weak bonding between the S-Mo-S layers in the MoS_2 structure [18]. This results in a random stacking layer structure, thus an increase of the lattice spacing [16]. Moreover, the broadening of the (002) peak indicates nanoscale crystals and some disorder in the crystals [19].

The TEM cross-section images of S7 is displayed in figure 4(a). The multilayer structure is well-defined with distinct interfaces. The white regions are DLC layers with a thickness of ~17 nm, while the dark regions are MoS_2 layers with ~83 nm thickness. The interfaces between the two types of layers show somewhat blurring that is caused by diffusion between DLC and MoS_2 components, which is shown in figure 4(b). In figure 4(b), the DLC layer is amorphous, while in MoS_2 layer the arrangement of MoS_2 basal pane is parallel to the interface in some degree accompanying with some defects and distortion regions. The curve of the interface contributes to the wave-like morphology of MoS_2 plane in turn. In addition, there are several types of crystal defects spotted in figure 4(c), such as bending defects (labeled B) where the basal plane is bended, fork defects (labeled F) where the basal plane forks into two, insetted defects (labeled I) where one plane insects between two others as well as

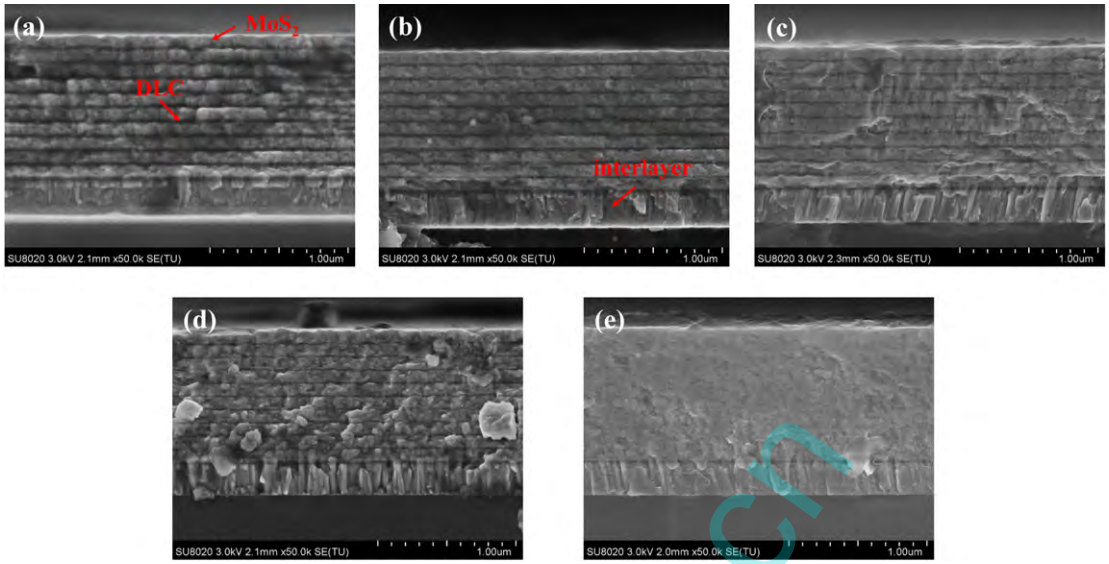

Figure 2. The cross-sectional FESEM images of the as-deposited coatings: (a) S3—DLC/MoS_2 = 1:3; (b) S5—DLC/MoS_2 = 1:5; (c) S7—DLC/MoS_2 = 1:7; (d) S9—DLC/MoS_2 = 1:9; (e) MoS_2—MoS_2 monolayer coating.

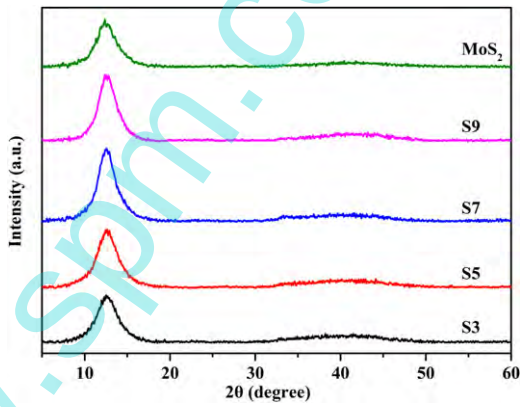

Figure 3. GIXRD patterns of coatings: (a) S3—DLC/MoS_2 = 1:3; (b) S5—DLC/MoS_2 = 1:5; (c) S7—DLC/MoS_2 = 1:7; (d) S9—DLC/MoS_2 = 1:9; (e) MoS_2—MoS_2 monolayer coating.

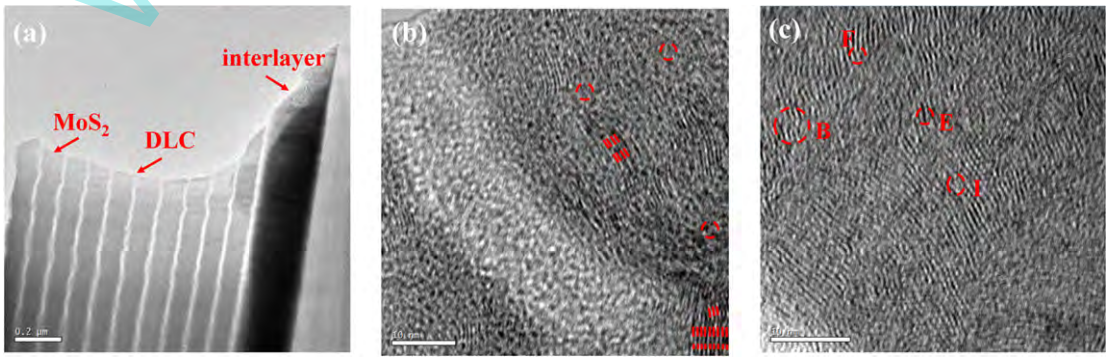

Figure 4. The cross-sectional TEM image of S7: (a) multilayer structure; (b) the parallel basal planes marked by parallel dash lines and defects marked by round dash lines; (c) several crystal defects.

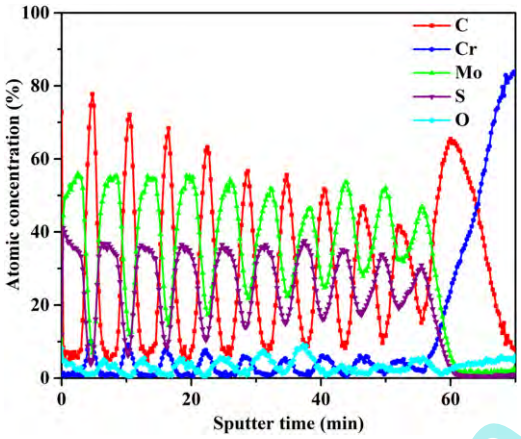

Figure 5. Atomic concentration-depth profile of $(DLC/MoS_2)_{10}$ multilayer coating with a modulation ratio DLC:MoS_2 = 1:7.

expanded lattices (labeled E), in which some defects are observed by others, too [20]. Deposition rate has a significant influence on the orientation of MoS_2 basal planes [21]. Optimal deposition rate will yield the strongest (002) orientation. Slower deposition rate not only inhibits (002) growth due to desorbing of incident atoms but also increases the concentration of contaminant atoms disrupting (002) growth. Considering the plentiful defects (O substitutions, vacancies) on the basal plane, the chemical reactivity of (002) plane is enhanced. Hence, a more intense competition occurs between (002) basal plane and (100) edge plane, which generates the morphology shown in figures 4(b) and (c).

Auger electron spectroscopy has become the most common method in sputter depth profiling for surface analysis. During the sputter process, the change of composition and topography in the surface introduced by beam/sample interactions will influence the depth resolution, so do other factors like ion-bombardment-induced roughing, atomic mixing and electron escape depth [22]. The direct evidence is a decreasing amplitude of the elemental concentration with increasing sputtering time. The AES depth profile of S7 in figure 5 shows the concentration-depth profile of a typical multilayered structure. Overall, the alternating of Mo and S-enriched and C-enriched layers demonstrates the presence of a well-defined multilayered structure. Compared with S, the higher concentration of Mo in the spectra is probably due to the instruments and the differences of sensitivity factors between element and compound. The synchronization of Mo and S concentration is a result of the preferential resputtering of S with respect to Mo [3]. In fact, the deposition speeds of MoS_2 and C are almost same in our experiments, so the periodical undulation of O concentration originates from the different reactivity of O in the different deposition stage, as O substitution is often seen in sputtered MoS_2 coatings. Generally, the depth resolution will decrease with the increasing sputter depth, which is due to preferential sputtering and the variation of sputtering yield with orientation and surface roughening *et al* [23], which leads to the decrease of the concentration amplitude. The diffusion in the interface is a result of the impact of sputtering particles, because Cr content is about zero in MoS_2 layer. This result is consistent with the observation in figure 4(b).

3.2. Mechanical properties

In order to evaluate the mechanical properties of the DLC/MoS_2 multilayer and MoS_2 monolayer coatings, nanoindentation experiments were performed and corresponding results are shown in figure 6. Typically, the hardness of transition metal dichalcogenides (TMD) is in the range of 0.3 to 2 GPa, which is much lower than that of DLC [24]. However, the hardness of sputtered MoS_2 is 7.9 GPa in our tests, which is much higher than that of the traditional MoS_2. A dense and compact structure contributes to the high hardness of MoS_2 film accompanying with the crystal defects which inhibit the dislocation motion [25]. Similarly, in the building of MoST film, a high hardness is ascribed to the lattice distortion of MoS_2 [26]. The combination MoS_2 and DLC shows weak influence on mechanical properties. The elastic modulus of coatings is in the range of 114 GPa to 97 GPa, and the hardness varies from 8.6 GPa to 7.9 GPa. Overall, the elastic modulus decreases with the thickness of DLC layer slightly, while the hardness varies little with irregular fluctuation.

3.3. Damp heat test

Figure 7 illustrates the XPS fine scan spectra obtained from S7 and MoS_2 monolayer coatings as-deposited and after the damp heat test. In figure 7(a), the Mo 3d spectrum recorded on the as-deposited MoS_2 monolayer coating surface exhibits two peaks at 228.7 eV and 231.8 eV, corresponding to the Mo $3d_{5/2}$ and Mo $3d_{3/2}$ in MoS_2. The peaks observed at 227.9 eV and 231.0 eV can be identified to be the Mo $3d_{5/2}$ and Mo $3d_{3/2}$ spectra

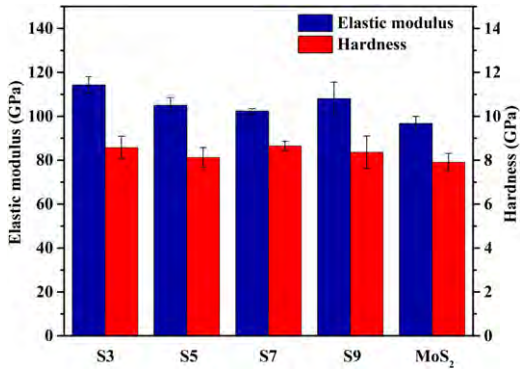

Figure 6. The elastic modulus and hardness of all coatings: (a) S3—DLC/MoS_2 = 1:3; (b) S5—DLC/MoS_2 = 1:5; (c) S7—DLC/MoS_2 = 1:7; (d) S9—DLC/MoS_2 = 1:9; (e) MoS_2—MoS_2 monolayer coating.

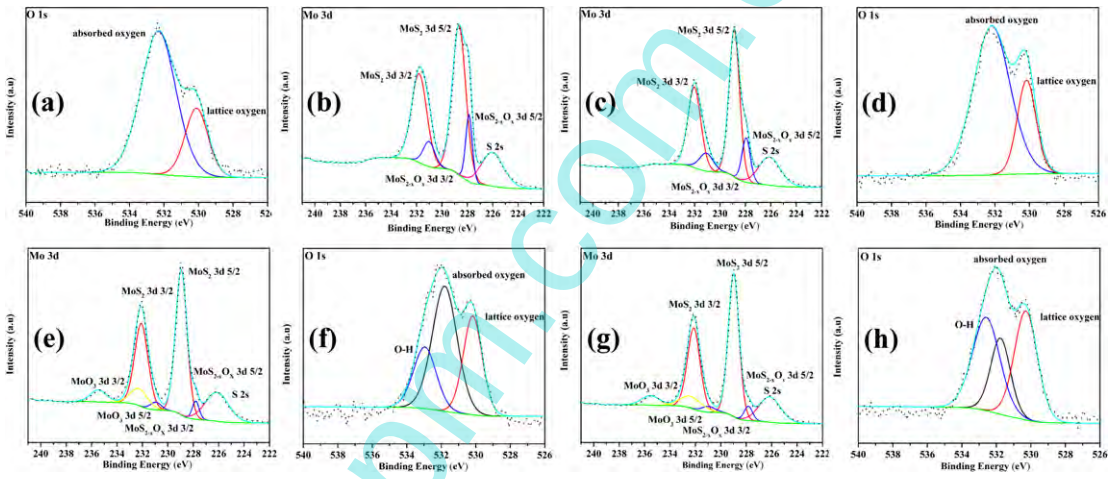

Figure 7. XPS spectra of the as-deposited MoS_2 monolayer coating and S7 accompanying with the results after the damp heat test: (a) Mo 3d of as-deposited MoS_2 monolayer coating; (b) O 1s of as-deposited MoS_2 monolayer coating; (c) Mo 3d of as-deposited S7; (d) O 1s of as-deposited S7; (e) Mo 3d of MoS_2 monolayer coating after damp heat test; (f) O 1s of MoS_2 monolayer coating after damp heat test; (g) Mo 3d of S7 after damp heat test; (h) O 1s of S7 after damp heat test.

line in $MoS_{2-x}O_x$, which is different from the results of others who assigned the peaks to MoS, as the sputtered-deposited 'MoS_2' films are composed of pure MoS_2 phase and $MoS_{2-x}O_x$ phase due to oxygen substituted for sulfur into the MoS_2 hexagonal lattice [27–29]. In addition, no peak around 336 eV is found, which suggests the amount of MoO_3 is too few to detect. The O 1 s spectrum in figure 7(b) can be fitted into two peaks. The peak located at 532.3 eV can be ascribed to chemically adsorbed oxygen, and the peak located at 530.1 eV suggests the Mo-O bonds which verify the oxygen substitution rather than surface oxidation [30, 31]. The spectra of S7 in figures 7(c) and (d) are similar to that of MoS_2 monolayer coating. MoS_2 monolayer and S7 coatings were stored at 40 °C, 80% relative humidity for 1 month to investigate the change in composition. The differences are presence of peaks from MoO_3 accompanying with the decreasing intensity of peaks correspond to $MoS_{2-x}O_x$. Based on the FESEM and XRD observations, the surface of MoS_2 layer consists of densely fine particles with numerous boundaries and certain edge sites directly exposed to the environment. Though a dense structure can inhibit the penetration of O_2 which leads to the limited oxidation of edge sites of MoS_2, it should be noted that the MoO_3 is mainly from the transformation of $MoS_{2-x}O_x$, as the portion of MoO_3 plus the residual $MoS_{2-x}O_x$ is almost equal to that of $MoS_{2-x}O_x$ in as-deposited coating in terms of the content of Mo, which is shown in table 2. This result suggests that the chemical reactivity of $MoS_{2-x}O_x$ is higher than that of the edge sites of MoS_2. Moreover, a new peak around 533 eV appear in the spectra of O 1s in figures 7(f) and (h), which can be ascribed to the signal of absorbed water as samples are stored in high humidity environment for a month before XPS characterization [32].

Table 2. The content of different Mo compounds in MoS_2 monolayer coating and S7 as-deposited and after damp heat test.

Sample	MoS_2	MoS_xO_{2-x}	MoO_3
MoS_2 (as-deposited)	80.70%	19.30%	—
S7 (as-deposited)	82.30%	17.70%	—
MoS_2 (after damp heat test)	80.50%	6.20%	13.30%
S7 (after damp heat test)	79.88%	5.98%	14.14%

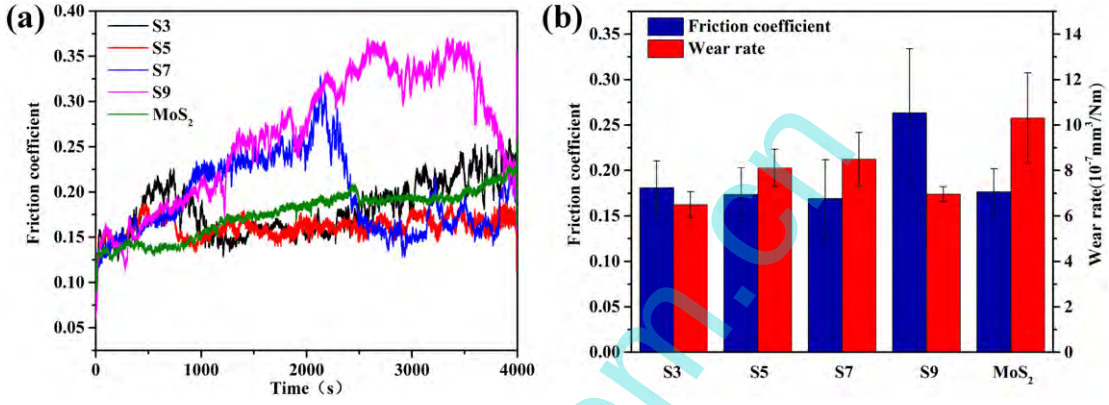

Figure 8. The tribological performance of all coatings: (a) the friction coefficients; (b) the average friction coefficients and wear rates.

3.4. Friction and wear properties

MoS_2 is vulnerable to humidity, which results in poor tribological properties. When tribological tests are performed at ~90% relative humidity a steady-state friction coefficient for MoS_2 is not realistic. Figure 8(a) presents the friction coefficients which show obvious fluctuation as the test proceeds. The friction coefficients of S3 increases continuously after the running-in period, while a steady stage appears for S5. With the thickness of DLC layer decreasing, a more severe running-in is observed. As seen in S7 and S9, the running-in periods need more time and the friction coefficients are more unstable, which is followed by a sharply decrease later. Different from others, the friction coefficient of MoS_2 monolayer coating increases steadily without great fluctuation. The mean friction coefficients and wear rates are shown in figure 8(b). From the results it can be concluded that an introduction of DLC layer is beneficial to reduce the wear, which is at the sacrifice of running-in period and a steady friction coefficient. As the thickness of DLC layer increase, the wear rates decrease, too. Meanwhile, the friction coefficient keeps low and steady.

To obtain more insights into the friction and wear mechanism of the coatings in high humidity condition, Raman spectra of as-deposited coatings, wear tracks and wear scars of MoS_2 monolayer and S7 coatings were carried out. As shown in figure 9(a), there are only two prominent peaks at ~373 cm^{-1} (E^1_{2g} mode) and ~402 cm^{-1} (A_{1g} mode) of spectra of as-deposited MoS_2 monolayer coating. The in-plane opposite vibration of two S atoms with respect to the Mo atom is responsible for E^1_{2g} mode, and the A_{1g} mode is attributed to the out-of-plane vibration of S atoms in opposite directions [33]. The absence of Raman signals (750–1000 cm^{-1}) due to MoO_3 indicates the content of MoO_3 is below the detection limit, which is consistent with the result of XPS [34]. The spectrum of the wear track is similar to that of as-deposited coatings without obvious peak corresponding to MoO_3. However, the presence of a sharp peak at ~920 cm^{-1} suggests the formation and accumulation of the oxidation product of MoS_2 on the surface of counterpart during the test. Compared with the spectrum of wear track of MoS_2 monolayer coating, a weak peak appearing between 1300 and 1700 cm^{-1} which belongs to the overlapping of D and G bands for DLC suggests the existence of carbon on the surface [35]. While much stronger signals originating from DLC in the wear scar of S7 indicate the enrichment of carbon which is beneficial to reduce wear.

After the tribological tests, the wear tracks and scars were observed by profilometer and SEM. The corresponding compositions were measured by EDS. As shown in figure 10(a), there are many rough grooves on the wear track of MoS_2 monolayer coating, which indicates abrasive wear due to the formation of harder particles. More specific information of the wear track is shown in the partial enlarged drawing. Delamination of the film on sides of grooves suggests the brittleness of MoS_2 and weak resistance to crack propagation, which is also supported by the deep and narrow valley depicted in the wear track profile. In addition, as shown in figure 10(b), a transfer film is formed with loose wear debris around the middle zone on the counterpart. In

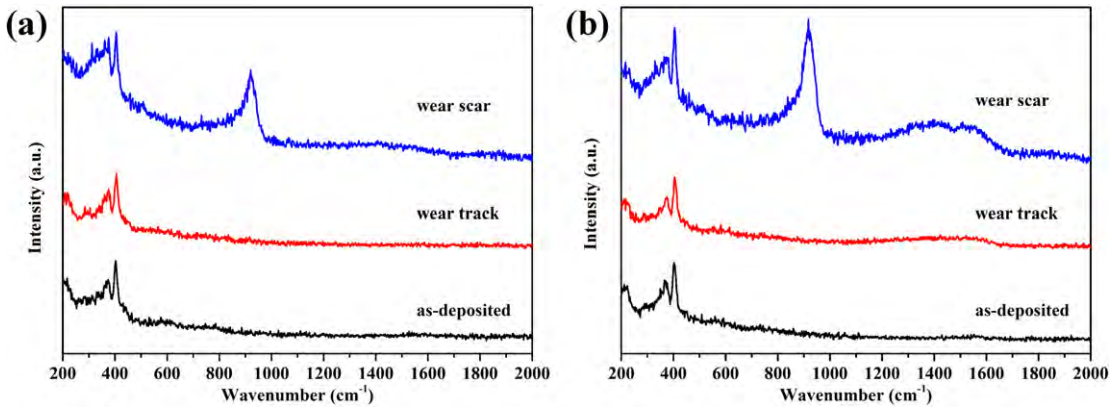

Figure 9. Raman spectra of as-deposited coatings, wear tracks and wear scars: (a) MoS_2 monolayer coating; (b) S7—DLC/MoS_2 = 1:7.

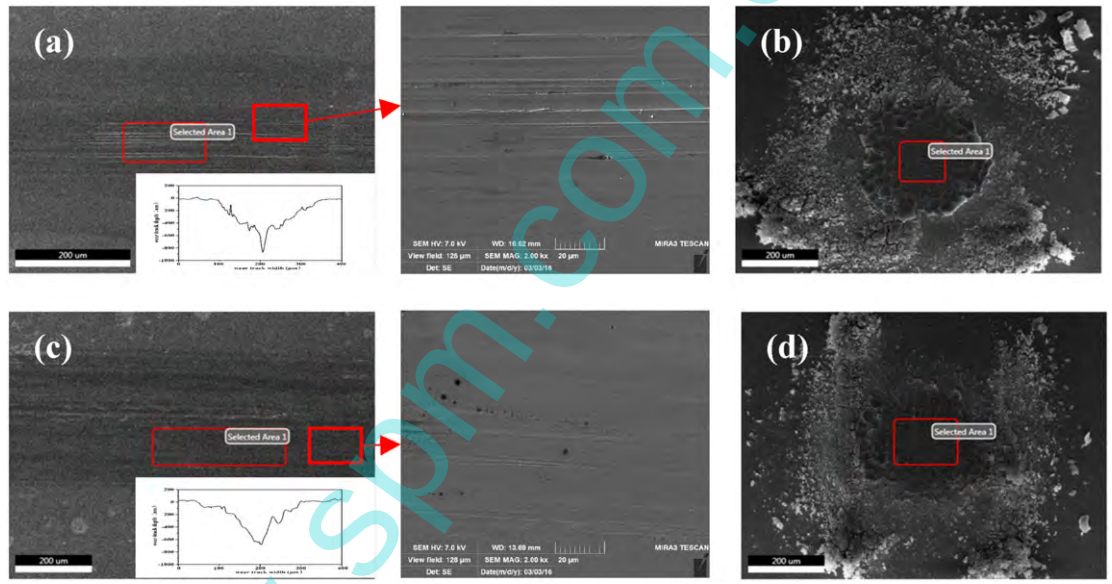

Figure 10. The wear tracks and transfer films of MoS_2 monolayer coating and S7: (a) wear track of MoS_2 monolayer coating; (b) transfer film of MoS_2 monolayer coating; (c) wear track of S7; (d) transfer film of S7. The red boxes with 'selected area' in the figures are the observed areas of EDS.

figure 10(c), the number of grooves of S7 are fewer, but the width is larger and more wear debris are distributed outside of the wear track. In the enlarged picture, a smoother surface with the absence of delamination of the film is observed. The wear track profile of S7 presents a shallower valley, which may be due to the enhanced carrying capacity and crack resistance resulting from the multilayer interfaces. The transfer film of S7 in figure 10(d) is surrounded by wear debris out of sliding directions, unlike a round-like shape of MoS_2 monolayer coating. This implies that the incorporation of DLC layer accelerates the gather of wear debris to form transfer film, which can also be demonstrated by the larger area of packed transfer film. Meanwhile, the accumulation produces more concentrated grooves with the feature of fewer numbers. The EDS results of labeled selected areas of wear tracks and wear scars are shown in table 3. Due to the formation of MoO_3, the counterballs are greatly worn, leaving in abundant Fe on the wear tracks. The failing detection of O suggests the good oxidation resistance of sample MoS_2 monolayer coating and S7. Even though oxidation happens, it's limited to the superficial part and doesn't penetrate to the bulk. However, a number of O is observed in their transfer films, indicating the oxidation of MoS_2 and the generation of iron oxide. The difference in O content between the wear track and transfer film may be explained by the density, for the film beneath the wear track being densely packed and the transfer film being loose with many macro boundaries. In the wear track of S7, C becomes the most abundant element by a replacement of Fe, and a lower S/Mo ratio is found, too. In the transfer film of MoS_2 monolayer coating, the content of Mo plus S is much less than that in S7 which is also accompanied with a preference of C. However, the same loose structure results in the excessive oxidation of the transfer film of S7.

Table 3. EDS of related elements of wear tracks and transfer films.

	Element analyses				
	Mo	S	O	C	Fe
wear track (MoS_2)	17.0%	31.5%	0.0%	—	51.5%
transfer film (MoS_2)	6.4%	13.1%	32.1%	—	48.4%
wear track (S7)	15.4%	20.5%	0.1%	38.0%	26.0%
transfer film (S7)	2.8%	6.1%	29.5%	14.2%	47.4%

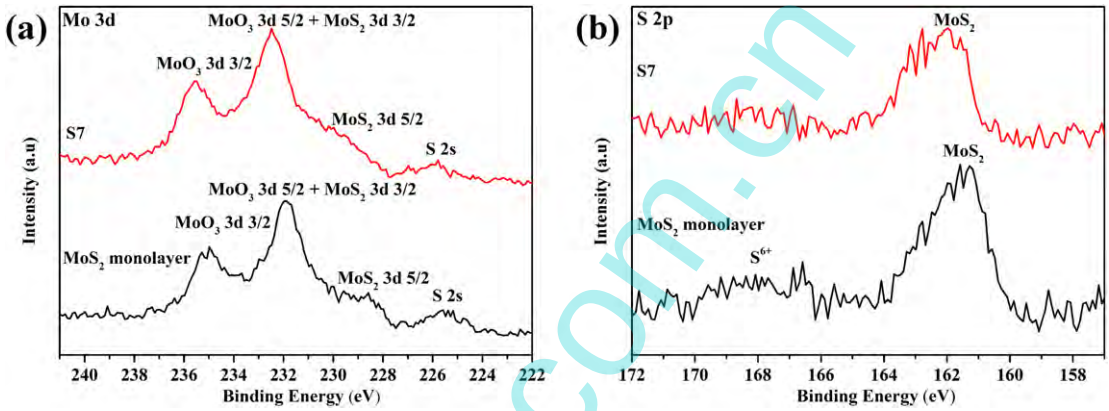

Figure 11. XPS spectra of the transfer film of MoS_2 monolayer coating and S7: (a) Mo 3d; (b) S 2p.

From the analysis above, we can get that the oxidation happens mainly in the transfer film during the tribological test. The introduction of DLC layer leads to the abundance of C which play a role in stabilizing the transfer film and reducing the wear.

To further explore the interaction of friction interface, the surfaces of transfer films were characterized by XPS and corresponding results are shown in figure 11. The peaks around 365.5 eV corresponding to MoO_3 are easily observed and the main source of XPS signals. While the peaks from MoS_2 are hard to distinguish. This indicates that the surface of wear scars is mainly composed of MoO_3 and the interface interaction occurred between MoO_3 and the coating. In figure 11(b), the peaks around 168 eV are originated from the S^{6+}, which suggests the oxidation reaction below occurs.

$$2MoS_2 + 4H_2O + 9O_2 - 2MoO_3 + 4H_2SO_4 \quad (1)$$

The sputtered-deposited 'MoS_2' films are mixed of pure MoS_2 phase and $MoS_{2-x}O_x$ phase [29]. Edge sites at steps within basal planes, along with the domain boundaries, are active sites vulnerable to oxidation [36]. Though the MoS_2 are oxidized at room temperature, the oxides removed by sliding lead to a negligible effect on the friction coefficient [5]. In sliding process, MoS_2 wear debris are transferred to the counterpart. When the environment humidity increases, though the contribution of water to MoS_2 oxidation is limited, more adsorbed water changes the shear strength of the interface, which results in an increase in friction [37]. The adsorption of water on defect sites has a tendency to form H-bonded network which can greatly increase the interface interaction [38]. At low humidity, the dimerization of N_2 and H_2O disturbs the network's formation. As the humidity increases, the interaction of N_2 and H_2O mainly occurs in the atmosphere, not at the defect sites, so a water linkage is formed. The friction of MoS_2 at ambient temperature relates to not only the amount of water in the environment but also the amount of diffused water in the bulk [5]. Water gradually penetrates into the bulk as the tests proceed. This phenomenon can increase the friction and wear, too. The incorporation of carbon reduces the portion of MoO_3 and the scale of H-bonded network, therefore the wear rate of multilayer is lower than that of MoS_2 monolayer coating.

4. Conclusion

A series of DLC/MoS_2 multilayer and MoS_2 monolayer coatings were fabricated by closed-field unbalanced magnetron sputtering system. The coatings show (002) orientation with many defects observed in TEM images. The modulus ratios have little influence on the hardness and elastic modulus. There is a certain degree of oxygen doped into MoS_2 layer forming the $MoS_{2-x}O_x$ phase which is easier to be oxidized in damp heat test and leads to a degraded performance. The incorporation of DLC layer can moderately decrease the wear rate compared with the MoS_2 monolayer coating, indicating promising potentials to enhance the performance in atmospheric environment. The better tribological properties of multilayer coatings are attributed to a reduced portion of MoO_3 and the H-bonded network inhibited by carbon.

Acknowledgments

The authors are grateful to the National Natural Science Foundation of China (Grant No. 21373249 and 51322508).

References

[1] Yang J-F, Parakash B, Hardell J and Fang Q-F 2012 Tribological properties of transition metal di-chalcogenide based lubricant coatings *Front. Mater. Sci.* **6** 116–27
[2] Zhang X, Han W P, Wu J B, Milana S, Lu Y, Li Q Q, Ferrari A C and Tan P H 2013 Raman spectroscopy of shear and layer breathing modes in multilayer MoS_2 *Phys. Rev.* B **87** 115413
[3] Lauwerens W, Wang J, Navratil J, Wieërs E, D'haen J, Stals L M, Celis J P and Bruynseraede Y 2000 Humidity resistant MoS_x films prepared by pulsed magnetron sputtering *Surf. Coatings Technol.* **131** 216–21
[4] Fleischauer P D 1984 Effects of crystallite orientation on environmental stability and lubrication properties of sputtered MoS_2 thin films *A S L E Trans.* **27** 82–8
[5] Khare H S and Burris D L 2014 Surface and subsurface contributions of oxidation and moisture to room temperature friction of molybdenum disulfide *Tribol. Lett.* **53** 329–36
[6] Ding X, Zeng X T, He X Y and Chen Z 2010 Tribological properties of Cr- and Ti-doped MoS_2 composite coatings under different humidity atmosphere *Surf. Coatings Technol.* **205** 224–31
[7] Vierneusel B, Schneider T, Tremmel S, Wartzack S and Gradt T 2013 Humidity resistant MoS_2 coatings deposited by unbalanced magnetron sputtering *Surf. Coatings Technol.* **235** 97–107
[8] Li H, Zhang G and Wang L 2016 Low humidity-sensitivity of MoS_2/Pb nanocomposite coatings *Wear* **350-351** 1–9
[9] Wang D, Chang C and Ho W 1999 Microstructure analysis of MoS_2 deposited on diamond-like carbon films for wear improvement *Surf. Coatings Technol.* **111** 123–7
[10] Hilton M R, Bauer R, Didziulis S V, Dugger M T, Keem J M and Scholhamer J 1992 Structural and tribological studies of MoS_2 solid lubricant films having tailored metal-multilayer nanostructures *Surf. Coatings Technol.* **53** 13–23
[11] Renevier N M, Lobiondo N, Fox V C, Teer D G and Hampshire J 2000 Performance of MoS_2/metal composite coatings used for dry machining and other industrial applications *Surf. Coatings Technol.* **123** 84–91
[12] Teer D G 2001 New solid lubricant coatings *Wear* **251** 1068–74
[13] Robertson J 2002 Diamond-like amorphous carbon *Mater. Sci. Eng. R Reports* **37** 129–281
[14] Erdemir A and Donnet C 2006 Tribology of diamond-like carbon films: recent progress and future prospects *J. Phys. D. Appl. Phys.* **39** R311–27
[15] Kim Y J, Byun T J, Lee H Y and Han J G 2008 Effect of bilayer period on CrN/Cu nanoscale multilayer thin films *Surf. Coatings Technol.* **202** 5508–11
[16] Rigato V, Maggioni G, Boscarino D, Sangaletti L, Depero L, Fox V C, Teer D and Santini C 1999 A study of the structural and mechanical properties of Ti-MoS_2 coatings deposited by closed field unbalanced magnetron sputter ion plating *Surf. Coatings Technol.* **116-119** 176–83
[17] Simmonds M C, Savan A, Van Swygenhoven H, Pflüger E and Mikhailov S 1998 Structural, morphological, chemical and tribological investigations of sputter deposited MoS_x/metal multilayer coatings *Surf. Coatings Technol.* **108–109** 340–4
[18] Moser J and Lévy F 1994 Random stacking in MoS_2 – x sputtered thin films *Thin Solid Films* **240** 56–9
[19] Yang X, Fu W, Liu W, Hong J, Cai Y, Jin C, Xu M, Wang H, Yang D and Chen H 2014 Engineering crystalline structures of two-dimensional MoS_2 sheets for high-performance organic solar cells *J. Mater. Chem.* A **2** 7727
[20] Dunn D N, Seitzman L E and Singer I L 1997 The origin of an anomalous, low 2θ peak in x-ray diffraction spectra of MoS_2 films grown by ion beam assisted deposition *J. Mater. Res.* **12** 1191–4
[21] Muratore C and Voevodin A A 2009 Control of molybdenum disulfide basal plane orientation during coating growth in pulsed magnetron sputtering discharges *Thin Solid Films* **517** 5605–10
[22] Hofmann S 2003 Advances in sputter depth profiling using AES *Surf. Interface Anal.* **35** 556–63
[23] Hofmann S, Erlewein J and Zalar A 1977 Depth resolution and surface roughness effects in sputter profiling of NiCr multilayer sandwich samples using Auger electron spectroscopy *Thin Solid Films* **43** 275–83
[24] Polcar T and Cavaleiro A 2011 Review on self-lubricant transition metal dichalcogenide nanocomposite coatings alloyed with carbon *Surf. Coatings Technol.* **206** 686–95
[25] Vaz F, Cerqueira P, Rebouta L, Nascimento S M C, Alves E, Goudeau P, Rivière J P, Pischow K and De Rijk J 2004 Structural, optical and mechanical properties of coloured TiN_xO_y thin films *Thin Solid Films* **447–448** 449–54
[26] Fox V C, Renevier N, Teer D G, Hampshire J and Rigato V 1999 The structure of tribologically improved MoS_2-metal composite coatings and their industrial applications *Surf. Coatings Technol.* **116–119** 492–7
[27] Wang X, Xing Y, Ma S, Zhang X, Xu K and Teer D G 2007 Microstructure and mechanical properties of MoS_2/titanium composite coatings with different titanium content *Surf. Coatings Technol.* **201** 5290–3

[28] Qin X, Ke P, Wang A and Kim K H 2013 Microstructure, mechanical and tribological behaviors of MoS_2-Ti composite coatings deposited by a hybrid HIPIMS method *Surf. Coatings Technol.* **228** 275–81
[29] Fleischauer P D and Lince J R 1999 A comparison of oxidation and oxygen substitution in MoS_2 solid film lubricants *Tribol. Int.* **32** 627–36
[30] Qiu H, Pan L, Yao Z, Li J, Shi Y and Wang X 2012 Electrical characterization of back-gated bi-layer MoS_2 field-effect transistors and the effect of ambient on their performances *Appl. Phys. Lett.* **100** 123104
[31] Cai Y, Yang X, Liang T, Dai L, Ma L, Huang G, Chen W, Chen H, Su H and Xu M 2014 Easy incorporation of single-walled carbon nanotubes into two-dimensional MoS_2 for high-performance hydrogen evolution *Nanotechnology* **25** 465401
[32] Díaz C, Lavayen V and O'Dwyer C 2010 Single-crystal micro/nanostructures and thin films of lamellar molybdenum oxide by solid-state pyrolysis of organometallic derivatives of a cyclotriphosphazene *J. Solid State Chem.* **183** 1595–603
[33] Li H, Zhang Q, Yap C C R, Tay B K, Edwin T H T, Olivier A and Baillargeat D 2012 From bulk to monolayer MoS_2: evolution of Raman Scattering *Adv. Funct. Mater.* **22** 1385–90
[34] Gu L, Ke P, Zou Y, Li X and Wang A 2015 Amorphous self-lubricant MoS_2-C sputtered coating with high hardness *Appl. Surf. Sci.* **331** 66–71
[35] Paik N 2005 Raman and XPS studies of DLC films prepared by a magnetron sputter-type negative ion source *Surf. Coatings Technol.* **200** 2170–4
[36] Gardos M N 1988 The synergistic effects of graphite on the friction and wear of MoS_2 films in air *Tribol. Trans.* **31** 214–27
[37] Zhao X and Perry S S 2010 The Role of Water in Modifying Friction within MoS_2 Sliding Interfaces *ACS Appl. Mater. Interfaces* **2** 1444–8
[38] Gardos M N 1995 Anomalous wear behavior of MoS_2 films in moderate vacuum and dry nitrogen *Tribol. Lett.* **1** 67–85